Thermodynamic Assessment of the Co-Mo System

A. Davydov and U.R. Kattner

(Submitted 12 March 1998; in revised form 3 August 1998)

Experimental thermochemical and phase diagram data for the Co-Mo system were assessed. A consistent thermodynamic description, using a Redlich-Kister model for the solution phases and sublattice and line-compound models for the intermetallics, was obtained, and it agreed well with the critically evaluated experimental data. Several variations of the sublattice model for the σ and μ phases were compared with the traditional models used for these phases in other systems. Measured data indicate an abrupt decrease of the terminal Mo solubility in the fcc (Co) phase with decreasing temperature. This behavior was reproduced well by inclusion of the magnetic contribution to the Gibbs energy of the fcc phase. Addition of the magnetic term also led to the prediction of a fcc (Co) miscibility gap, and a high-temperature stability region of the paramagnetic cph (Co) phase.

1. Introduction

The Co-Mo system is an important constituent subsystem of many Co- and Ni-base superalloys. Cobalt and Mo act as solid-solution strengtheners in Ni- and Co-base alloys, respectively. Addition of Co to Ni-base materials provides improved solid solubility of additives within the supersaturated matrix. Because fabrication and processing of superalloys involves the interaction of liquid/solid and solid/solid phases, the knowledge of the equilibrium phase diagram of the relevant superalloy system is important. The reliability of predicting phase equilibria in multicomponent superalloys relies largely on the accuracy of the descriptions of the constituent binary systems. Therefore, a thermodynamic reassessment of the Co-Mo system with respect to experimentally determined phase diagram and thermochemical data is necessary.

The only available description of the Co-Mo system [78Kau] gives a simplified phase diagram with all the intermetallic phases modeled as line compounds, in spite of the σ ("Co$_2$Mo$_3$") and μ ("Co$_7$Mo$_6$") phases exhibiting substantial homogeneity ranges of approximately 3 and 7 at.% Mo, respectively. The most comprehensive evaluations of phase diagram and thermochemistry data for the Co-Mo system were published in [80Bre] and [93Pre]. Both of these reviews, although based on complete and up-to-date experimental literature, depicted an undefined high-temperature stability limit for the ferromagnetic cph (Co) phase. They also failed to define the phase boundaries and crystallographic relation between the two compositionally close and structurally identical paramagnetic cph (Co) and θ ("Co$_9$Mo$_2$") phases.

This article reports a new thermodynamic analysis of the Co-Mo system, utilizing CALPHAD procedures for the calculation of phase diagrams and thermochemistry by using the software packages BINGSS, BINFKT [77Luk], and Thermo-Calc [85Sun].

A. Davydov and **U.R. Kattner,** Metallurgy Division, National Institute of Standards and Technology, 100 Bureau Dr., Stop 8555, Gaithersburg, MD 20899. (A. Davydov is also at the Department of Chemical Engineering, University of Florida, Gainesville, FL 32611.)

2. Evaluation of the Experimental Data

Table 1 summarizes the experimental data available for the Co-Mo system and the investigative techniques used. The last column indicates whether the measured values were used in the assessment.

2.1 Phase Diagram Data

The Co-Mo phase diagram is shown in Fig. 1. This system contains total of eight phases: four solution phases: liquid, cph (Co), fcc (Co), and a bcc (Mo) terminal solid solutions, plus four intermetallics: θ ("Co$_9$Mo$_2$"), ε ("Co$_3$Mo"), μ ("Co$_7$Mo$_6$"), and σ ("Co$_2$Mo$_3$"). The Co-base solid solutions include low-temperature ferromagnetic and high-temperature paramagnetic phase fields, denoted in Fig. 1 as α, α′ and β, β′ for the cph (Co) and the fcc (Co) phases, respectively.

For the whole compositional range, the liquidus curve was determined with good agreement by [13Ray], [53Met], and [63Qui]. As for the solid phases, a controversy still exists over the stability limits of the para-cph (Co) solid solution and its relation to the high-temperature θ phase: both phases have identical crystal structures and very similar lattice parameters as shown in Table 2. In the early works of [28Tak] and [32Kos], it was assumed that the cph (Co) phase field extended into the Co-Mo system up to 1273 K, dissolving almost 20 at.% Mo. In later interpretations [35Syk, 53Met, 63Qui, 74Hei, 75Gus] the stability of the cph phase was limited to 970 ± 150 K with a maximum solubility of only several at.% Mo. In these latter representations, the Co-rich cph phase containing 16 to 18 at.% Mo existed as an isolated θ phase, stable between 1290 and 1473 K. Because the cph (Co) and θ phases are structurally identical and have close compositions and because further clarification of the existence of the θ phase as a separate compound is lacking, the authors have accepted a description similar to the case of the Co-Cr system, in which the high-temperature Co-rich phase with the cph structure was treated as a paramagnetic cph (Co) phase [97Kus]. Following this interpretation, the cph (Co) and θ phases are described as Co-base cph solid solutions with two separate stability fields: the ferro-cph (Co) region, located in the Co-rich corner of the diagram below about 800 K, and the para-cph (Co), stable in

the limited temperature-composition range of 1291 to 1473 K at 16 to 19 at.% Mo.

The fcc (Co) solvus was studied extensively [28Tak, 32Kos, 35Syk, 63Qui, 70Kra, 74Hei, 75Gus, 75Kat, 81Tak]. Although the high-temperature fcc phase boundary is well established, there is a significant amount of scatter in the data with respect to the solubility of Mo in the fcc (Co) at temperatures below 1000 to 1200 K. Several authors [28Tak, 32Kos, 63Qui, 70Kra] found a gradual reduction in the terminal solubility of Mo in the fcc (Co) phase with decreasing temperature, while others [35Syk, 74Hei, 75Gus] found a stronger decrease in Mo solubility below about 1200 K. Using x-ray diffraction (XRD) and microprobe analysis, [81Tak] detected an abrupt change in the fcc (Co) solvus line at about 1150 K and showed that this anomaly is caused by the magnetic transformation in this phase. The effect of magnetic transformation on the fcc (Co) phase boundary was also demonstrated in evaluations of the Co-W [89Fer] and Co-Cr [97Kus] systems. For both Co-W and Co-Cr systems, asymmetric fcc (Co) miscibility gaps were predicted. These miscibility gaps, shaped as a sharp horn, protrude along the Curie temperature line and separate two fcc compositions: a Co-rich ferromagnetic phase and a Cr-rich (or W-rich) paramagnetic phase. As the determination of such narrow miscibility gaps can be experimentally difficult, this article explores the possibility of forming immiscible areas in the fcc (Co) phase in the Co-Mo system by thermodynamic analysis of the fcc solvus line and of the magnetic properties of this phase.

The phase boundary of the bcc (Mo) terminal solid solution was determined in [63Qui] and [74Hei] at high and low temperatures, respectively. The latter study established relatively low solubility limits of Co in the bcc (Mo) phase compared to [63Qui]. For example, extrapolating the bcc (Mo) solvus line from [74Hei] to the peritectic temperature of 1893 K yielded the value of the bcc (Mo) phase boundary at about 96 at.% Mo, while the experimental point from [63Qui] at this temperature was 92 at.% Mo. In this assessment, the bcc (Mo) phase boundary data determined in [63Qui] on high-temperature annealed alloys were given higher weight than the [74Hei] data, which are from kinetically limited studies on diffusion couples.

The homogeneity ranges of all the intermetallic compounds in the system were systematically investigated in [74Hei]. According to this study, the θ phase (or the para-cph (Co) solid solution, as defined in this work) is homogeneous from 17 to 19 at.% Mo, the ε phase from 23.5 to 25 at.% Mo, and the μ phase from 41.5 to 48.5 at.% Mo. The range of the σ phase was not well established, but was located within the limits of 60 to 65 at.% Mo. For the above intermetallics, this work accepts the [63Qui] temperature-stability limits, except for the lower limit of the σ phase that was extended from 1523 to 1273 K, as reported in both [74Hei] and [75Kat]. The peritectoid decomposition of the ε phase was corrected from 1298 K as estimated in

Table 1 Summary of the experimental data in the Co-Mo system

Type of data	Method	Composition, at.% Mo	Temperature, K	Data used	Ref
Liquidus, solidus	TA	0-55	1600-1800	Yes	[13Ray]
Solvus, T_c	DL, MT, MG	0-40	700-1300	Yes	[28Tak]
	DL, MG	0-35	700-1200	Yes(a)	[32Kos]
Liquidus, solidus, solvus	TA, MT, RS	0-92	990-1900	Yes	[35Syk]
	TA, DL	0-25	1500-1700	Yes	[53Met]
	TA, MT, XRD	0-100	1100-2600	Yes	[63Qui]
Activity of Mo in alloys	emf	3-40	1170-1475	No	[65Dro]
Solvus	DL	0-5	700-950	Yes	[70Kra]
	MT, XRD, MP	0-100	1050-1580	Yes	[74Hei]
	MT	0-8	970-1230	Yes	[75Gus]
Activity of Mo in alloys	emf	3-85	1223-1423	Yes	[75Kat]
Heat of formation and C_p for μ phase	CL	48	773-1573	Yes(a)	[75Spe]
Solvus	XRD, MP	0-15	1020-1530	Yes	[81Tak]
Heat of formation for μ and σ phases	CL	48, 64	1473, 1523	No	[83Kub]

CL, calorimetry; DL, dilatometry; emf, electromotive force measurements; MG, magnetic measurements; MT, metallography; MP, microprobe analysis; TA, thermal analysis; XRD, x-ray diffraction. (a) Not all the data were used in the optimization.

Table 2 Crystal structure and lattice parameter data of the cph (Co) and θ phases

Phase	Structure	Type	Space group	Parameters a	c	Ref
cph (Co)	cph	Mg	$P6_3/mmc$	2.567(a)	4.113(a)	[93Pre]
θ	cph	Mg	$P6_3/mmc$	2.597	4.212	[63Qui]

(a) Extrapolated to 18 at.% Mo

[63Qui] to the more accurate value of 1319 K from [28Tak]. The uncertainties of these characteristic temperatures for the intermetallic compounds were averaged in this work to ±10 K by comparing all the available data and evaluating the experimental methods listed in Table 1.

The only experimental measurements of the Curie temperature (T_c) of the fcc (Co) phase were conducted by [28Tak] and [32Kos]. The concentration dependence of T_c is shown in Fig. 2 and reveals a significant negative deviation from linearity. The T_c values from [32Kos] are 15 to 25% lower than those from [28Tak] and were assigned lower weight in the assessment because of the many discrepancies between the phase transformation measurements in [32Kos] and those in other sources.

2.2 Thermochemical Data

Table 1 summarizes thermodynamic experimental data reported in the literature including enthalpy of formation meas-

urements for the intermetallics [75Spe, 83Kub] and the activity of molybdenum in the (Co,Mo) alloys [65Dro, 75Kat].

Using a high-temperature adiabatic calorimeter, [75Spe] determined the enthalpy of formation for the μ phase containing 48 at.% Mo. The resulting $\Delta_f H$ values, measured at 973 and 1573 K, were –4160 and –4380 J/mol-at, respectively. This work was followed by calorimetric measurements of the heats of formation for the μ and σ phases at 1473 and 1523 K, respectively [83Kub]. The latter study revealed several nonequilibrium thermal transformations in the intermetallics, not verified in other works, such as a transition in the σ phase at 1514 K, where according to Fig. 1 no phase change should occur. This raised questions about the procedure of sample equilibration in [83Kub] and prompted the rejection of the above data from the assessment.
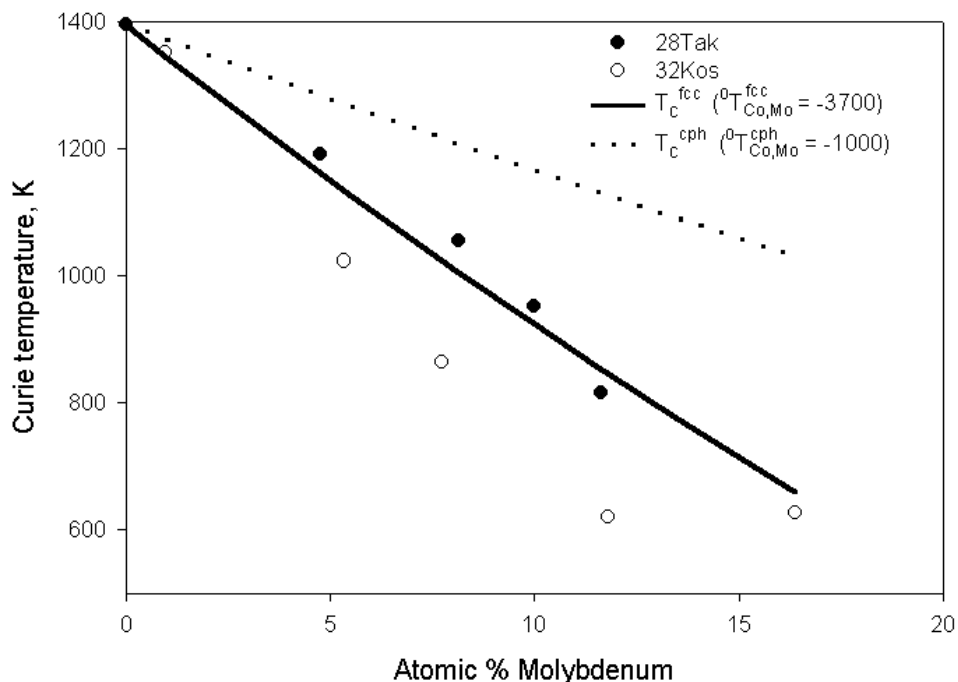
Thermodynamic activities of the cph (Co) solid solution were derived in [65Dro] from emf measurements between 1170 and 1475 K for alloys containing 3 to 40 at.% Mo. The results of this work, flawed by computation errors, were later
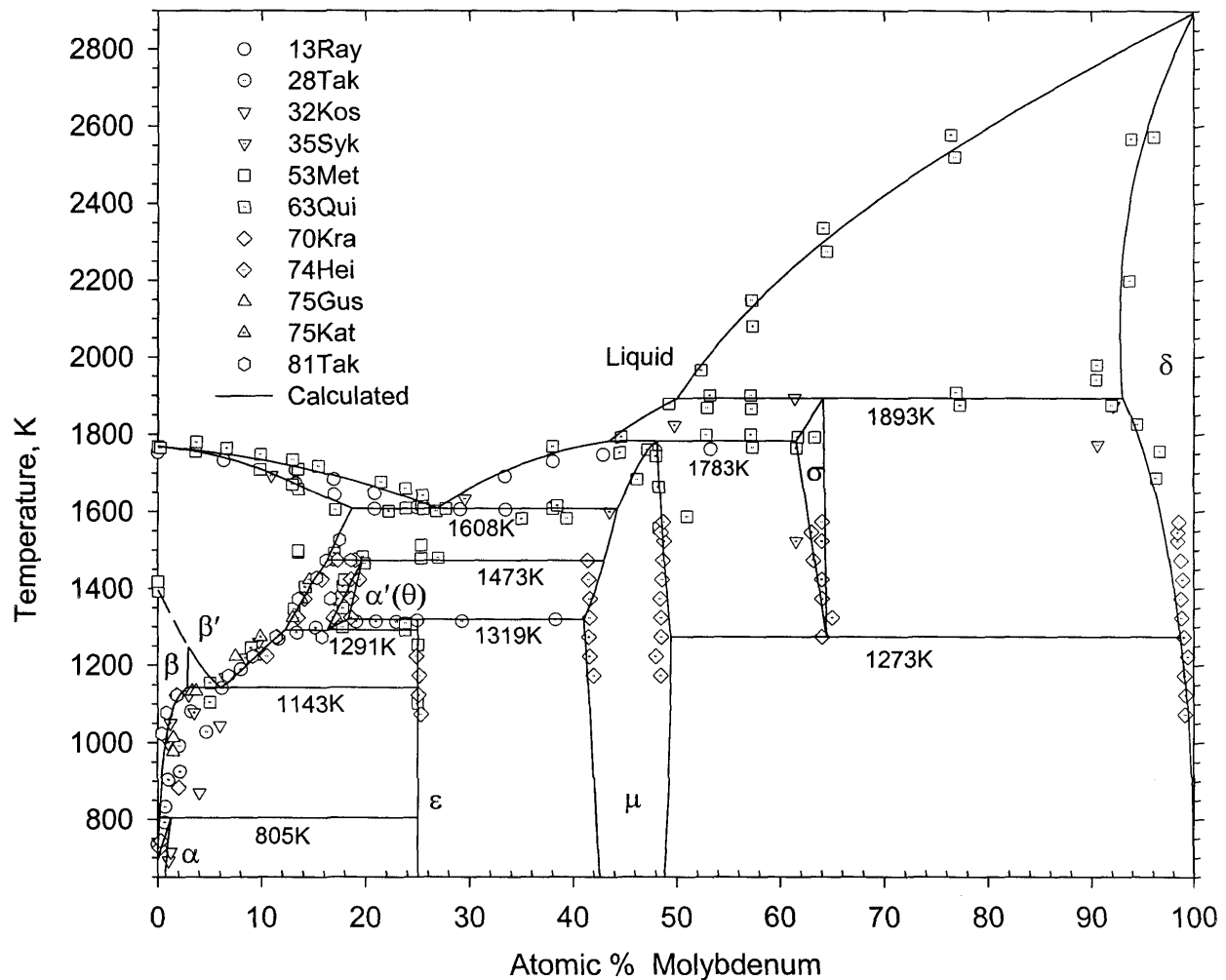

Fig. 1 Experimental and calculated phase diagram for the Co-Mo system: α, ferro-cph (Co); α′, para-cph (Co) (= θ, see text); β, ferro-fcc (Co); β′, para-fcc (Co); δ, bcc (Mo); ε, μ, and σ, intermetallic compounds

corrected by one of the coauthors in [78Rez]. Utilizing a similar type of emf cell with oxide electrolytes, [75Kat] measured molybdenum activity in the whole concentration range at temperatures between 1223 and 1423 K. The resulting activities are plotted in Fig. 3 and show a significant discrepancy be-

tween the values of [65Dro] and [75Kat] at compositions above 10 at.% Mo. As is discussed in section 3.2 of this article, the data from [65Dro] were found to be incompatible with the phase diagram data and were therefore excluded from the assessment. Although integral free energy, enthalpy, and entropy

Fig. 2 Curie temperature T_c for the fcc (Co) and cph (Co) phases: symbols, experimental data for the fcc (Co); lines, calculated from Eq 11
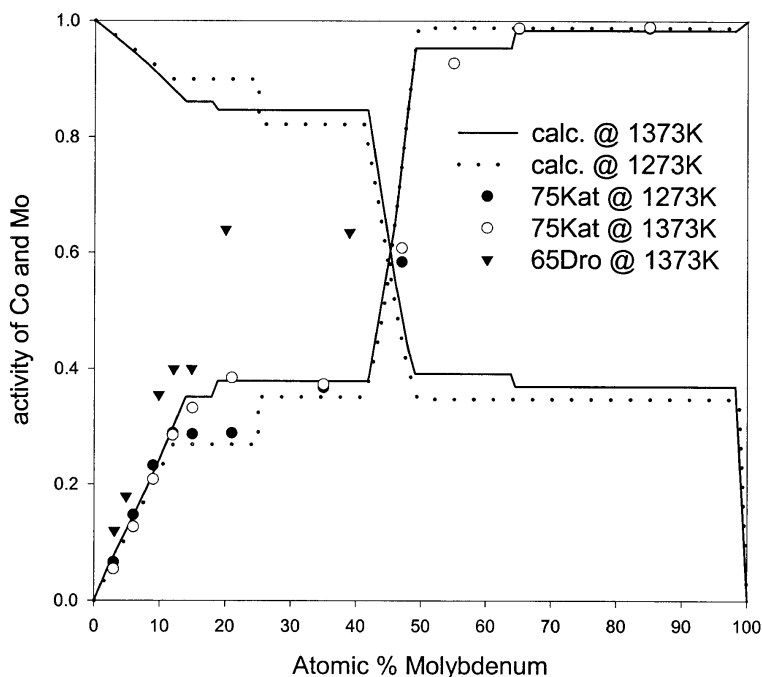
Fig. 3 Thermodynamic activities of Co and Mo at 1273 and 1373 K

of formation values of the intermetallic compounds were derived and reported in [65Dro] and [75Kat], these computed values tend to be very prone to accumulated errors. Therefore, only the experimental emf data, shown in Fig. 4 and converted to the partial Gibbs energy values of Mo, were used in the assessment.

3. Thermodynamic Models

3.1 Analytical Descriptions of the Phases

Pure Components. Gibbs energy expressions for the components in their standard states are represented as follows:

$$G_i(T) - H_i^{SER} = A + BT + CT \ln T + DT^2 + ET^{-1} + FT^3 + IT^7 + JT^{-9}$$

$$(Eq\ 1)$$

where H_i^{SER} are the enthalpy values for components in their stable forms at 1 atm and 298.15 K. The values of the coefficients A through J are from the SGTE databank [91Din].

Solution Phases. The liquid phase, the (Co) and (Mo) solid solutions were modeled as disordered phases using a Redlich-Kister polynomial [48Red] to describe their excess Gibbs energies. The total Gibbs energy for the above phases is represented by the reference (ref), ideal (id), excess (ex), and the magnetic (magn) parts in terms of one mole of atoms:

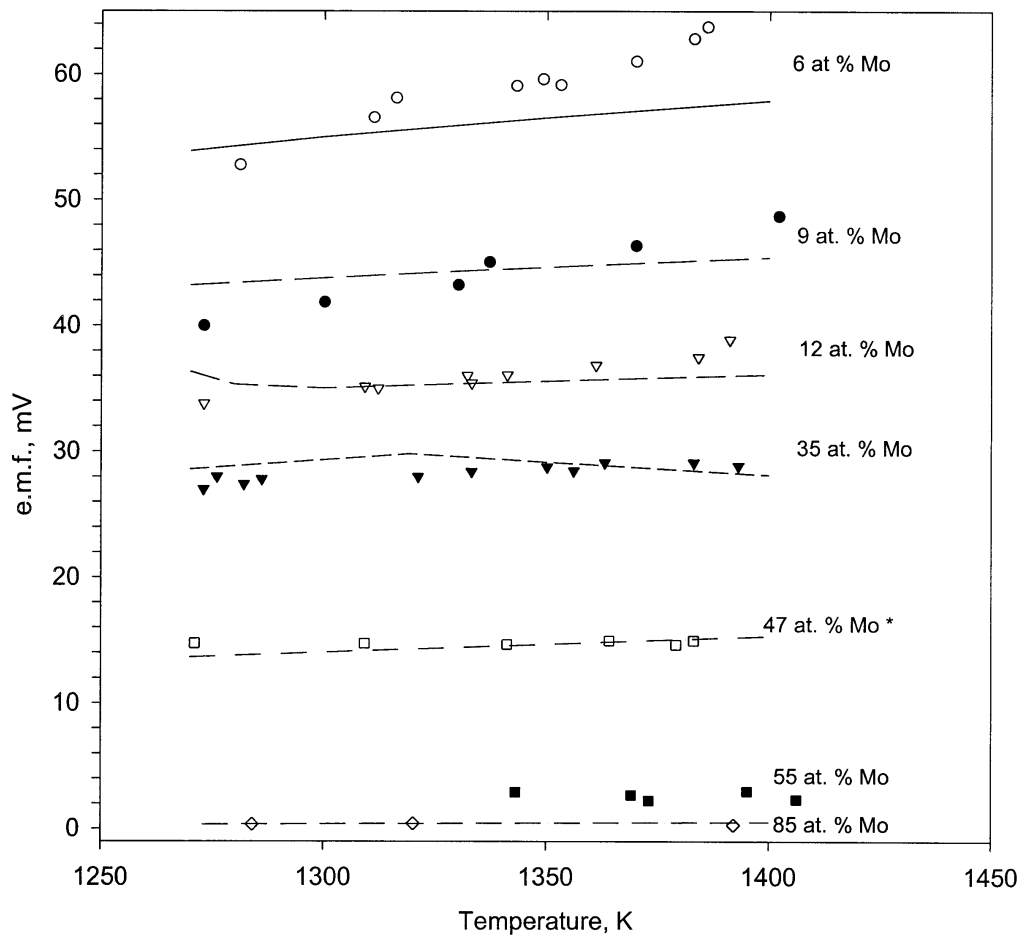$$G^{\Phi} = G^{ref,\Phi} + G^{id,\Phi} + G^{ex,\Phi} + G^{magn,\Phi} \qquad (Eq\ 2)$$

where

$$G^{ref,\Phi} = x_{Co}\ {}^0G_{Co}^{\Phi} + x_{Mo}\ {}^0G_{Mo}^{\Phi} \qquad (Eq\ 3)$$

$$G^{id,\Phi} = RT(x_{Co} \ln x_{Co} + x_{Mo} \ln x_{Mo}) \qquad (Eq\ 4)$$

$$G^{ex,\Phi} = x_{Co}\, x_{Mo}\ \Sigma^j L_{Co,Mo}^{\Phi}\, (x_{Co} - x_{Mo})^j \qquad (Eq\ 5)$$

The magnetic contribution $G^{magn,\Phi}$ to the Gibbs energy of the cph (Co), fcc (Co), and bcc (Mo) solution phases in ferromagnetic and paramagnetic states is described after [78Hil] and [91Din] as follows:

Fig. 4 Experimental [75Kat] and assessed emf data for the (Co,Mo) alloys. *, line is calculated for the 46 at.% Mo composition

$$G^{\mathrm{magn},\Phi} = RT\ln(\beta + 1)f(\tau) \qquad \text{(Eq 6)}$$

where $\tau = T/T_c$, T_c is the Curie temperature, and β is the effective magnetic moment per atom. The function $f(\tau)$ for both cph and fcc phases is given by:

$$f(\tau) = 1 - 0.86034\,\tau^{-1} - 0.17449\,\tau^3 - 0.007755\,\tau^9$$
$$- 0.001745\,\tau^{15} \text{ for } \tau \le 1 \qquad \text{(Eq 7)}$$

$$f(\tau) = -0.04269\,\tau^{-5} - 0.001355\,\tau^{-15} - 0.000285\,\tau^{-25} \text{ for } \tau > 1 \qquad \text{(Eq 8)}$$

and for the bcc phase it is described as:

$$f(\tau) = 1 - 0.90530\,\tau^{-1} - 0.15301\,\tau^3 - 0.006800\,\tau^9$$
$$- 0.001530\,\tau^{15} \text{ for } \tau \le 1 \qquad \text{(Eq 9)}$$

$$f(\tau) = -0.06417\,\tau^{-5} - 0.0020372\,\tau^{-15} - 0.000428\,\tau^{-25}$$
$$\text{for } \tau > 1 \qquad \text{(Eq 10)}$$

The concentration dependencies of the T_c and β are expressed as follows:

$$T_c^{\Phi} = x_{\mathrm{Co}}\,{}^0T_{\mathrm{Co}}^{\Phi} + x_{\mathrm{Co}}\,x_{\mathrm{Mo}}\,{}^0T_{\mathrm{Co,Mo}}^{\Phi} \qquad \text{(Eq 11)}$$

and

$$\beta^{\Phi} = x_{\mathrm{Co}}\,{}^0\beta_{\mathrm{Co}}^{\Phi} + x_{\mathrm{Co}}\,x_{\mathrm{Mo}}\,{}^0\beta_{\mathrm{Co,Mo}}^{\Phi} \qquad \text{(Eq 12)}$$

where Φ denotes cph (Co), fcc (Co), or bcc (Mo) phases, ${}^0T_{\mathrm{Co}}^{\Phi}$ and ${}^0\beta_{\mathrm{Co}}^{\Phi}$ refer to the pure Co values, and ${}^0T_{\mathrm{Co,Mo}}^{\Phi}$ and ${}^0\beta_{\mathrm{Co,Mo}}^{\Phi}$ are adjustable parameters, evaluated as described in section 3.2. Negative values of T_c^{Φ} and β^{Φ} indicate the antiferromagnetic state and must be divided by –3 for the fcc and cph phases and by –1 for the bcc phase in order to be used with Eq 6 to 8 [82Her]. It should also be noted that T_c^{Φ} and β^{Φ} must change sign at the same composition so that they are physically meaningful [89Fer].

Intermetallic Compounds. The ε phase crystallizes in an ordered cph structure of the Ni_3Sn ($D0_{19}$) prototype. Because it reveals only a narrow homogeneity range, its description was simplified to a line compound model with Co_3Mo stoichiometry. Its Gibbs energy is expressed in J/mol by the following equation referring to the pure elements in their non-magnetic states:

$$G^{\varepsilon} = 3\,{}^0G_{\mathrm{Co}}^{\mathrm{cph}} + {}^0G_{\mathrm{Mo}}^{\mathrm{bcc}} + \Delta_f G^{\varepsilon} \qquad \text{(Eq 13)}$$

where $\Delta_f G^{\varepsilon}$ is the Gibbs energy of formation of this compound and is represented as $\Delta_f G^{\varepsilon} = a + bT$, with adjustable a and b parameters.

The remaining two intermetallics, the μ and the σ phases, were described by a compound energy formalism [81Sun] to accommodate their substantial homogeneity ranges. Ideally, a complete thermodynamic description of these phases should include five crystallographic sites (sublattices) in each com-

pound [96Ans]. However, such a description would have too many adjustable parameters to fit with experimental data. For the σ phase, the ideal site occupancy can be expressed as $Co_2Mo_4Mo_8Co_8Mo_8$, or in general form as: $B_2A_4A_8B_8A_8$. The following two simplifications of this model have been employed: model I $(A,B)_8(A)_4(A,B)_{18}$ by [87And] was used in the Co-Cr [97Kus], Fe-Cr [87And], Fe-Mo [88Fer], and Mn-V [91Hua] systems, and model II $(A,B)_{10}(A)_4(A,B)_{16}$ [82Her] was used to describe σ phases in the Fe-V [83And], Fe-Mo [82Fer], and Al-Ta [90Kat, 96Du] systems. In model I, the first, third, and fifth sites in $B_2A_4A_8B_8A_8$ were combined to form the $(A,B)_{18}$ sublattice, and the second and fourth sites formed the $(A)_4$ and the $(A,B)_8$ sublattices, respectively. In the modified model II, the third and fifth sites were combined into the $(A,B)_{16}$ sublattice, the second site formed the $(A)_4$ sublattice, and the first and the fourth sites were allowed to mix on the $(A,B)_{10}$ sublattice.

The x-ray single crystal study of the σ phase in the Co-Mo system revealed the following distributions on the five sublattices (in percent of Co occupation): $(100)_2(0)_4(12.5)_8(100)_8(12.5)_8$ [63For]. This prompted the authors to favor model II for their assessment, modified as $(B)_{10}(A)_4(A,B)_{16}$ and equivalent to the $(Co)_{10}(Mo)_4(Co,Mo)_{16}$ formula. However, because model I is commonly used to describe σ phases in metal systems, they also tested the $(Co)_8(Mo)_4(Co,Mo)_{18}$ model for this article. The alternative representations of the σ phase by models I and II allow the flexibility to interchangeably use either of these descriptions for future extrapolations into higher-order systems.

For the μ phase, the ideal five sublattice model is $B_1A_2A_2A_2B_6$, where A and B denote Mo and Co, respectively. Following the recommendations of [97Ans] and ensuring that the model would cover the whole homogeneity range of the μ phase, between about 41 and 49 at.% Mo, the ideal description can be reduced to the following three principal formulas: model III $(Co,Mo)_7(Co,Mo)_6$, model IV $(Co,Mo)_7(Mo)_2(Co,Mo)_4$, and model V $(Co,Mo)_1Mo_4(Co,Mo)_2(Co)_6$. These models have the same ideal Co_7Mo_6 stoichiometry but different hypothetical end-member compounds, thus accommodating different limits of the homogeneity range for the μ phase. Model IV continues to be the most commonly used in the literature. It was employed to describe the μ phases in Co-W [89Fer], Fe-Mo [88Fer], Fe-Nb [90Hua], and Fe-W [87Gus]. Model III was also successfully utilized in Fe-Nb, Fe-Ta [94Coe], and Ni-Nb [96Bol] assessments, while model V, which is closest to the ideal five sublattice model, was used only in the Co-Nb system [97Har]. As with the σ phase modeling, all three of the above models were tested and compared in the assessment as described in sections 3.2, and 4.

A general description of models I and II for the σ phase and models III, IV, and V for the μ phase considers four sublattices, where one is occupied only by Co, another only by Mo, and the remaining two are occupied by a substitutional solution, $(Co)_{a^i}(Co,Mo)_{a^{ii}}(Mo)_{a^{iii}}(Co,Mo)_{a^{iv}}$. The stoichiometric number of each sublattice is determined by the selected model description. The general equation for the Gibbs energy is constructed in a similar way as Eq 2 for the solution phases and is:

$$G^\Phi = A(x_{\mathrm{Co}}\,{}^0G_{\mathrm{Co}}^{\mathrm{cph}} + x_{\mathrm{Mo}}\,{}^0G_{\mathrm{Mo}}^{\mathrm{bcc}})$$
$$+ RT\{a^{\mathrm{ii}}(y_{\mathrm{Co}}^{\mathrm{ii}}\ln y_{\mathrm{Co}}^{\mathrm{ii}} + y_{\mathrm{Mo}}^{\mathrm{ii}}\ln y_{\mathrm{Mo}}^{\mathrm{ii}})$$
$$+ a^{\mathrm{iv}}y_{\mathrm{Co}}^{\mathrm{iv}}\ln y_{\mathrm{Co}}^{\mathrm{iv}} + y_{\mathrm{Mo}}^{\mathrm{iv}}\ln y_{\mathrm{Mo}}^{\mathrm{iv}}\} + y_{\mathrm{Co}}^{\mathrm{ii}}y_{\mathrm{Co}}^{\mathrm{iv}}\,\Delta_{\mathrm{f}}G_{\mathrm{Co:Co:Mo:Co}}$$
$$+ y_{\mathrm{Co}}^{\mathrm{ii}}y_{\mathrm{Mo}}^{\mathrm{iv}}\,\Delta_{\mathrm{f}}G_{\mathrm{C\alpha Co:Mo:Mo}} + y_{\mathrm{Mo}}^{\mathrm{ii}}y_{\mathrm{Co}}^{\mathrm{iv}}\,\Delta_{\mathrm{f}}G_{\mathrm{Co:Mo:Mo:Co}}$$
$$+ y_{\mathrm{Mo}}^{\mathrm{ii}}y_{\mathrm{Mo}}^{\mathrm{iv}}\,\Delta_{\mathrm{f}}G_{\mathrm{C\alpha Mo:Mo:Mo}}$$
$$+ y_{\mathrm{Co}}^{\mathrm{ii}}y_{\mathrm{Mo}}^{\mathrm{ii}}y_{\mathrm{Co}}^{\mathrm{iv}}\sum_{j=0}^{n_1}{}^jL_{\mathrm{Co:Co,Mo:Mo:Co}}(y_{\mathrm{Co}}^{\mathrm{ii}} - y_{\mathrm{Mo}}^{\mathrm{ii}})^j$$
$$+ y_{\mathrm{Co}}^{\mathrm{ii}}y_{\mathrm{Mo}}^{\mathrm{ii}}y_{\mathrm{Mo}}^{\mathrm{iv}}\sum_{j=0}^{n_2}{}^jL_{\mathrm{Co:Co,Mo:Mo:Mo}}(y_{\mathrm{Co}}^{\mathrm{ii}} - y_{\mathrm{Mo}}^{\mathrm{ii}})^j$$
$$+ y_{\mathrm{Co}}^{\mathrm{ii}}y_{\mathrm{Co}}^{\mathrm{iv}}y_{\mathrm{Mo}}^{\mathrm{iv}}\sum_{j=0}^{n_3}{}^jL_{\mathrm{Co:Co:Mo:Co,Mo}}(y_{\mathrm{Co}}^{\mathrm{iv}} - y_{\mathrm{Mo}}^{\mathrm{iv}})^j$$
$$+ y_{\mathrm{Mo}}^{\mathrm{ii}}y_{\mathrm{Co}}^{\mathrm{iv}}y_{\mathrm{Mo}}^{\mathrm{iv}}\sum_{j=0}^{n_3}{}^jL_{\mathrm{Co:Mo:Mo:Co,Mo}}(y_{\mathrm{Co}}^{\mathrm{iv}} - y_{\mathrm{Mo}}^{\mathrm{iv}})^j \quad \text{(Eq 14)}$$

where a^{i}, a^{ii}, a^{iii}, and a^{iv} are the stoichiometric numbers of the sublattices with $A = a^{\mathrm{i}} + a^{\mathrm{ii}} + a^{\mathrm{iii}} + a^{\mathrm{iv}}$; $y_{\mathrm{Co}}^{\mathrm{ii}}$, $y_{\mathrm{Mo}}^{\mathrm{ii}}$, $y_{\mathrm{Co}}^{\mathrm{iv}}$, and $y_{\mathrm{Mo}}^{\mathrm{iv}}$ are the site fractions of element Co and Mo on sublattices ii and iv with $y_{\mathrm{Co}}^{\mathrm{ii}} + y_{\mathrm{Mo}}^{\mathrm{ii}} = 1$, $y_{\mathrm{Co}}^{\mathrm{iv}} + y_{\mathrm{Mo}}^{\mathrm{iv}} = 1$ and $(a^{\mathrm{i}} + a^{\mathrm{ii}}y_{\mathrm{Co}}^{\mathrm{ii}} + a^{\mathrm{iv}}y_{\mathrm{Co}}^{\mathrm{iv}})/A = x_{\mathrm{Co}}$, $(a^{\mathrm{ii}} + y_{\mathrm{Mo}}^{\mathrm{ii}} + a^{\mathrm{iii}} + a^{\mathrm{iv}}y_{\mathrm{Mo}}^{\mathrm{iv}})/A = x_{\mathrm{Mo}}$. The first term in Eq 14 corresponds to $G^{\mathrm{ref},\Phi}$, and the second term corresponds to $G^{\mathrm{id},\Phi}$ in Eq 2. The remaining terms correspond to the excess Gibbs energy term, $G^{\mathrm{ex},\Phi}$, in Eq 2. No magnetic contribution, $G^{\mathrm{magn},\Phi}$, to the Gibbs energy is considered for the σ or μ phases. The stoichiometric numbers a^{i} through a^{iv} of the sublattices in the individual model descriptions are given in Table 3. It should be noted that if the stoichiometric number a^{ii} for the sublattice allowing substitution is set to zero, the number of terms in Eq 14 is reduced accordingly.

3.2 Optimization of Model Parameters

The data marked "yes" in Table 1 were used for optimization of the Gibbs energy model parameters. The software packages BINGSS, BINFKT, and Thermo-Calc were used for both optimization and phase diagram calculation. In the optimization procedure, each set of data from Table 1 was assigned a certain weight based on the evaluated accuracy of the experimental method used, the validity of the results, and the com-

patibility with the other data sets. During the course of the optimization, some of the initial weights were adjusted to accommodate the overall data consistency. For example, the weights for the emf data from [75Kat] were reduced due to incompatibility of the emf measurements for the fcc (Co) phase with the solvus data for this phase, otherwise causing the fcc phase boundary to be shifted to higher Mo concentrations. Optimization of the coefficients in the Gibbs energy expressions for the solution phases and the compounds was carried out in several consecutive steps. In the first treatment, the initial parameter values were determined only for the solution phases from a hypothetical phase diagram, extrapolated from the equilibrium diagram with the assumption that no intermetallic phases are stable. To simplify the description and to reduce the number of adjustable parameters, the ${}^0T_{\mathrm{Co,Mo}}^\Phi$ and ${}^0\beta_{\mathrm{Co,Mo}}^\Phi$ (Φ = fcc, cph, bcc) coefficients were set to zero, assuming linearity of the T_{c}^Φ and β^Φ composition dependencies. Notably, at this preliminary assessment step, it was found that the emf values from [65Dro] appeared to be too high, thus conflicting with the fcc (Co) phase boundary data. For this reason, the subset [65Dro] was excluded from the assessment.

Once preliminary values for the solution phase parameters were obtained (with no more than two ${}^iL^\Phi$ parameters per phase), the intermetallic phases were introduced to the assessment. At this second stage, the para-cph (Co) phase was also added to the assessment. Phases μ, σ, and ε were treated as line compounds with initial $\Delta_{\mathrm{f}}G$ values determined in [75Spe] for the μ phase and evaluated in [80Bre] for all the other intermetallics. At the same time, parameters for the solution phases were readjusted except for the fixed zero values of ${}^0T_{\mathrm{Co,Mo}}^\Phi$ and ${}^0\beta$ (Φ = fcc, cph, bcc).

In the third step, the compound energy models were employed to accommodate the homogeneity ranges for the μ and σ phases. Because the ε phase has a narrow homogeneity region of less than 1.5 at.% Mo, only the line compound model was used for this phase description. The initial sublattice model for the μ phase was chosen as $(\mathrm{Co,Mo})_7(\mathrm{Co,Mo})_6$ (model III). The number of adjustable parameters in this model can be reduced by applying several assumptions. First, the parameters $\Delta_{\mathrm{f}}G_{\mathrm{Co:Co}}^{\mathrm{III}}$ and $\Delta_{\mathrm{f}}G_{\mathrm{Mo:Mo}}^{\mathrm{III}}$ represent the Gibbs energy of formation of pure Co and Mo in the virtual state of the μ phase. In compliance with the rationale given by [93Dup], [94Coe], and [96Bol], these quantities were fixed at 5000 J/mol-at. Secondly, the parameter $\Delta_{\mathrm{f}}G_{\mathrm{Co:Mo}}^{\mathrm{III}}$ represents the Gibbs energy of formation of the ideal $\mathrm{Co}_7\mathrm{Mo}_6$ stoichiometric composition and can be optimized by fitting to the available experimental data of [75Spe]. Finally, the $\Delta_{\mathrm{f}}G_{\mathrm{Mo:Co}}^{\mathrm{III}}$ parameter corresponds to the

Table 3 Stoichiometric numbers a^{i}, a^{ii}, a^{iii}, and a^{iv} of the sublattices in the different model descriptions of the σ and μ phases

| Phase | Model | Formula | Stoichiometric numbers | | | |
			a^{i}	a^{ii}	a^{iii}	a^{iv}
σ	I	$(\mathrm{Co})_8(\mathrm{Mo})_4(\mathrm{Co,Mo})_{18}$	8	0	4	18
	II	$(\mathrm{Co})_{10}(\mathrm{Mo})_4(\mathrm{Co,Mo})_{16}$	10	0	4	16
μ	III	$(\mathrm{Co,Mo})_7(\mathrm{Co,Mo})_6$	0	7	0	6
	IV	$(\mathrm{Co,Mo})_7(\mathrm{Mo})_2(\mathrm{Co,Mo})_4$	0	7	2	4
	V	$(\mathrm{Co})_6(\mathrm{Co,Mo})_1(\mathrm{Mo})_4(\mathrm{Co,Mo})_6$	6	1	4	6

Gibbs energy of formation of the Co_6Mo_7 virtual compound formed by filling both sublattices with antistructure defects. In accordance with [97Ans], the following equation can be applied to this term:

$$\Delta_f G_{Mo:Co}^{III} = \Delta_f G_{Co:Co}^{III} + \Delta_f G_{Mo:Mo}^{III} - \Delta_f G_{Co:Mo}^{III} \qquad \text{(Eq 15)}$$

As a result, only two independent parameters remain in model III: $^0L_{Co,Mo:*}^{III}$ and $^0L_{*:Co,Mo}^{III}$, where * denotes either Co or Mo. The authors assumed that the interaction between species on either sublattice is independent of the species occupying the other sublattice.

The same approach was applied to parameter evaluation for models IV and V for the μ phase. In addition, the optmized

Table 4 Models and their parameters optimized for the Co-Mo system

Phase	Model (Eq No.)	Parameter(a)	Coefficient(a) a_i	b_i
Liquid	Redlich-Kister (Eq 5)	$^0L_{Co,Mo}$	−87,020.2	43.036
		$^1L_{Co,Mo}$	6,523.4	2.012
cph α	Redlich-Kister (Eq 5, 11, 12)	$^0L_{Co,Mo}$	−29,315.7	23.755
		$^1L_{Co,Mo}$	−27,975.9	−1.936
		$^2L_{Co,Mo}$	24,698.3	0.000
		$^0T_{Co}, {}^0\beta_{Co}$	1,396	1.350
		$^0TCo_{,Mo}, {}^0\beta Co_{,Mo}$	−1,000	0.000
fcc β	Redlich-Kister (Eq 5, 11, 12)	$^0L_{Co,Mo}$	−29,557.1	10.953
		$^1L_{Co,Mo}$	−1,382.2	15.371
		$^2L_{Co,Mo}$	−18,135.4	0.000
		$^0T_{Co}, {}^0\beta_{Co}$	1,396	1.350
		$^0TCo_{,Mo}, {}^0\beta Co_{,Mo}$	−3,700	−3.578
bcc δ	Redlich-Kister (Eq 5, 11, 12)	$^0L_{Co,Mo}$	5,902.3	7.597
		$^1L_{Co,Mo}$	−17,675.9	0.000
		$^0T_{Co}, {}^0\beta_{Co}$	1,450	1.350
		$^0TCo_{,Mo}, {}^0\beta Co_{,Mo}$	−3,700	−3.445
ε	Line compound (Eq 13)	$\Delta_f G$	−47,009.6	20.816
σ	$(Co)_8(Mo)_4(Co,Mo)_{18}$ (Model I, Eq 14)	$\Delta_f G_{Co:Mo:Co}$	−318,839.1	286.332
		$\Delta_f G_{Co:Mo:Mo}$	−81,513.9	8.905
	$(Co)_{10}(Mo)_4(Co,Mo)_{16}$ (Model II, Eq 14)	$\Delta_f G_{Co:Mo:Co}$	−342,196.0	406.427
		$\Delta_f G_{Co:Mo:Mo}$	−106,690.3	−6.856
μ	$(Co,Mo)_7(Co,Mo)_6$ (Model III, Eq 14)	$\Delta_f G_{Co:Mo}$	−105,406.7	19.784
		$\Delta_f G_{Co:Co}$	65,000.0	0.000
		$\Delta_f G_{Mo:Mo}$	65,000.0	0.000
		$\Delta_f G_{Mo:Co}$	235,406.7	−19.784
		$^0LCo_{,Mo:Mo}$	−71,900.0	171.864
		$^0LCo_{,Mo:Co}$	−71,900.0	171.864
		$^0LCo:Co_{,Mo}$	−314,202.1	276.666
		$^0LMo:Co_{,Mo}$	−314,202.1	276.666
	$(Co,Mo)_7(Mo)_2(Co,Mo)_4$ (Model IV, Eq 14)	$\Delta_f G_{Co:Mo:Mo}$	−105,406.7	19.784
		$\Delta_f G_{Co:Mo:Co}$	−64,478.6	49.936
		$\Delta_f G_{Mo:Mo:Mo}$	65,000.0	0.000
		$\Delta_f G_{Mo:Mo:Co}$	105,928.1	30.152
		$^0LCo_{,Mo:Mo:Mo}$	−70,203.8	170.256
		$^0LCo_{,Mo:Mo:Co}$	−70,203.8	170.256
		$^0LCo:Mo:Co_{,Mo}$	−133,923.6	125.818
		$^0LMo:Mo:Co_{,Mo}$	−133,923.6	125.818
	$(Co)_6(Co,Mo)_1(Mo)_4(Co,Mo)_2$ (Model V, Eq 14)	$\Delta_f G_{Co:Co:Mo:Mo}$	−105,406.7	19.784
		$\Delta_f G_{Co:Co:Mo:Co}$	−130,245.8	57.602
		$\Delta_f G_{Co:Mo:Mo:Mo}$	−87,000.0	15.000
		$\Delta_f G_{Co:Mo:Mo:Co}$	−111,839.1	52.818
		$^0LCo:Co_{,Mo:Mo:Co}$	−8,416.5	13.433
		$^0LCo:Co_{,Mo:Mo:Mo}$	−8,416.5	13.433
		$^0LCo:Co:Mo:Co_{,Mo}$	−15,272.5	24.341
		$^0LCo:Mo:Mo:Co_{,Mo}$	−15,272.5	24.341

(a) The a_i and b_i coefficients for the G and L parameters are given in J/mol and J/mol · K, respectively; T_c in K; and β in Bohr magnetons.

value of $\Delta_f G_{Co:Mo}^{III}$ for model III was used for $\Delta_f G_{Co:Mo:Mo}^{IV}$ and $\Delta_f G_{Co:Mo:Mo}^{V}$ in models IV and V.

Both models for the σ phase contain two adjustable parameters related to Gibbs energies of formation of the hypothetical end-member phases: $Co_{26}Mo_4$ and Co_8Mo_{22} for model I, and $Co_{26}Mo_4$ and $Co_{10}Mo_{20}$ for model II, plus the Redlich-Kister terms from the excess Gibbs energy contribution. Because the experimental phase boundaries of the σ phase are not well defined, it was sufficient to describe the σ phase with only two parameters for each model and without introducing the Redlich-Kister terms. Further, it was desirable to keep an overall description of the Gibbs energy for the σ phase by models I and II as similar as possible during the optimization, so the models could be used interchangeably in extrapolations.

In the final assessment step, the nonlinear concentration dependencies of T_c^{Φ} and β^{Φ} (Φ = cph, fcc, bcc) were accounted for by introducing $^0T_{Co,Mo}^{\Phi}$ and $^0\beta_{Co,Mo}^{\Phi}$ nonzero coefficients in Eq 11 and 12. The only experimental data for T_c^{Φ} concentration dependence are known for the fcc (Co) phase as described in section 2.1 and are shown in Fig. 2. They were fit independently to Eq 11, yielding the value $^0T_{Co,Mo}^{fcc} = -3700$ K. The parameter $^0\beta_{Co,Mo}^{fcc}$ from Eq 12 was estimated following the empirical correlation between T_c^{fcc} and β^{fcc} suggested by [55Tau] and used by [89Fer] for the Co-W system description. This approximation implies that $\beta^{fcc} = 0$ at the same composition where $T^{fcc} = 0$, leading to the following equation:

$$^0\beta_{Co,Mo}^{fcc} = (^0\beta_{Co}^{fcc}/^0T_{Co}^{fcc}) \, ^0T_{Co,Mo}^{fcc} \qquad (Eq\ 16)$$

where the magnetic properties of pure Co are: $^0\beta_{Co}^{fcc} = 1.35$ and $^0T_{Co}^{fcc} = 1396$ K [91Din].

Lacking information on the magnetic properties of Co in the cph and bcc phases, it was first assumed that $^0T_{Co,Mo}^{cph} = ^0T_{Co,Mo}^{bcc} = ^0T_{Co,Mo}^{fcc}$ and that Eq 16 is also valid for the cph and bcc phases. While this description worked well for the bcc phase, it caused a compatibility problem between the resulting Gibbs energy expression for the cph phase and the reproducibility of the experimental para-cph (Co) phase boundary. Therefore, the initial value of –3700 for the $^0T_{Co,Mo}^{cph}$ parameter was readjusted during the optimization to –1000, so that the homogeneity range of the para-cph (Co) phase could be described satisfactorily. Because the expression $T_c^{cph} = 1396x_{Co} - 1000x_{Co}x_{Mo}$ remains positive at any given composition, there was no need for correlating β^{cph} and T_c^{cph} concentration behavior, as expressed in Eq 16. Therefore, with no experimental data available, the $^0\beta_{Co,Mo}^{cph}$ coefficient was set to zero.

After all the Gibbs energy expressions in the system were optimized, the calculated phase diagram revealed a problem in the Co-rich corner, where some equilibria involving the para-cph (Co) phase became stable. To ensure that only observed equilibrium phases are present in the diagram at temperatures above 200 K over the entire composition range, it was necessary to introduce a third composition term in the cph (Co) and fcc (Co) Gibbs energy descriptions. Adding the extra term, one for each phase, corrected the problem while making only slight changes to the existing model coefficients. The final list of model parameters (Table 4) was used to calcu-

late phase diagram and thermochemical properties (see Fig. 1 to 6 and Table 5).

4. Discussion and Results

Figure 1 is the calculated equilibrium phase diagram with all the experimental values used in the assessment. The two most distinctive differences between this work and previous evaluations [78Kau, 80Bre, 93Pre] are: (a) the peculiarity of the fcc (Co) solvus line and (b) the description of the para-cph (Co) solid solution, called the θ phase in all previous publications.

The fcc (Co) phase boundary exhibits an abrupt decrease in Mo solubility at temperatures below about 1150 K (Fig. 1), which is caused by the magnetic contribution to the Gibbs energy. Figure 5 illustrates that if the coefficient $^0T_{Co,Mo}^{fcc}$ in Eq 11 was set to zero, implying linear concentration dependence for T_c^{fcc}, then the solvus line would gradually decrease with lowering temperature. Setting $^0T_{Co,Mo}^{fcc}$ to –3700, however, not only allows a fit to both high- and low-temperature fcc (Co) solvus data, but also predicted the formation of a miscibility gap in the fcc (Co) phase. The width of this miscibility gap has a maximum of about 3 at.% Mo at the monotectoid temperature of 1143 K and gradually decreases toward the tricritical point at 1246 K. Such a ferro/para-fcc immiscible region, although predicted in several Co-base fcc alloys [82Ind, 89Fer, 97Kus], would be very difficult to detect experimentally: Co-V is the only Co-base binary system in which such a miscibility gap was observed [81Ind]. As in the Co-Mo system, Co-V exhibits a very strong decrease of T_c in the fcc (Co) phase with increasing solute content.

As shown in Fig. 1, cph (Co) solid solutions are represented by two homogeneous regions in the calculated phase diagram: the ferromagnetic α phase field with the maximum decomposition temperature of 805 K at 1.3 at.% Mo and the paramagnetic α' phase field, stable at high temperatures. The latter phase, called in the literature the compound θ, is calculated to be stable in the 1291 to 1473 K temperature interval within the homogeneity region of 16.4 to 19.6 at.% Mo. Based on the identical crystal structures of the cph (Co) and θ phases, and similarity with the Co-Cr system, this phase is described as the para-cph (Co). The calculated concentration dependence of the T_c^{cph} for this phase is shown in Fig. 2 by the dotted line. The less pronounced negative deviation from linearity, as opposed to T_c^{fcc} dependence, is not based on experimental data and is the result of trial-and-error fitting to achieve compatibility with experimental phase boundary data for para-cph (Co). Therefore, the concentration dependence of T_c^{cph} and β^{cph} should be considered highly uncertain.

Models III to V for the μ phase identically reproduced its homogeneity region throughout the whole temperature range. Models I and II for the σ phase fit the phase diagram data well within the experimental uncertainties, but yield slightly different σ phase boundaries (Fig. 6). Broader homogeneity limits from model I can be associated with the fact that this model allows wider homogeneity range of 13 to 73 at.% Mo, compared to 13 to 67 at.% Mo for model II. Models I and II and III to V adequately describe the system and can be used interchangeably. The preference may depend on the compatibility of these

models with other phase descriptions and on their ability to be extrapolated into the higher-order systems.

Calculated thermodynamic properties of the intermetallic phases are presented in Table 5 and are compared with the evaluated values, recommended in [80Bre]. Assessed entropies and enthalpies of formation for the intermetallics are in fair agreement, although the averaged $\Delta_f H_{298}$ and $\Delta_f S_{298}$ values of [80Bre] should be considered as less reliable, because they were derived solely from the emf data of [65Dro] and [75Kat]. As already mentioned, such derived quantities may accumulate errors not only from the experiment itself, but also from the scatter in the Gibbs energy temperature dependence and from the Gibbs energy values of the oxides involved in emf measurements. A direct calorimetric determination of the enthalpy of formation for the μ phase with 48 at.% Mo at 973
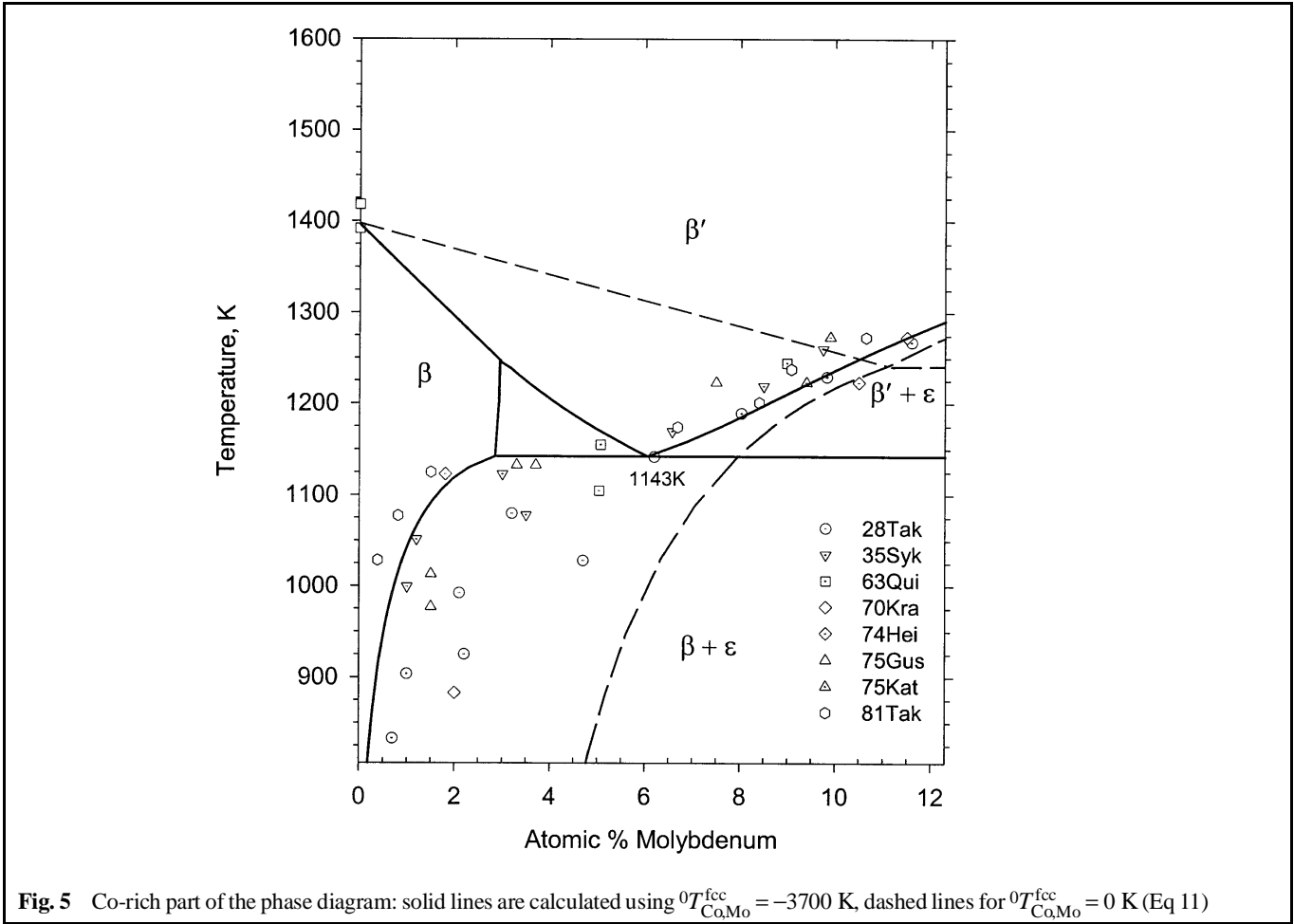
K $\Delta_f H_{973} = -4160$ J/mol-at [75Spe] is in excellent agreement with the calculated value of -4370 J/mol-at at this temperature.

Figure 4 is a comparison between the experimental emf data from [75Kat] used in the assessment, and the calculated emf temperature dependence for relevant compositions between 6 and 85 at.% Mo. In spite of the overall good fit to the experimental data, the weight for the emf data set in the assessment was intentionally reduced relative to the weight of the phase diagram data. This was necessary because the emf measurements for single-phase alloys with low Mo contents were in conflict with most of the fcc (Co) solvus data, causing the terminal fcc solubility field to be wider than its experimentally determined limits. The less satisfactory fit to the emf data points for the 3, 6, and 9 at.% Mo samples (with the former composition not included in Fig. 4) may be related to composi-

Table 5   Calculated thermodynamic properties of the intermetallic compounds

Phase	x, at.% Mo	T_{melt}, K	$\Delta_f H^{298}$, J/mol-at	$\Delta_f S^{298}$, J/mol-at · K	$\Delta_f H^{298}$ [80Bre], J/mol-at	$\Delta_f S^{298}$ [80Bre], J/mol-at · K
ε	25	1319(a)	−5360	0.1	−5300 ± 1200	−1.3 ± 0.8
μ	48	1783	−3530	2.4	−3800 ± 400	1.8 ± 0.8
σ	63	1893	−940	3.0	−1900 ± 2500	3.3 ± 1.2

(a) Peritectoid decomposition

Fig. 5   Co-rich part of the phase diagram: solid lines are calculated using $^0T^{fcc}_{Co,Mo} = -3700$ K, dashed lines for $^0T^{fcc}_{Co,Mo} = 0$ K (Eq 11)

tional inhomogeneity of the fcc (Co) alloys prepared by [75Kat]. It is likely, that for the same reason, it was difficult to reproduce the emf data set for the μ phase with 47 at.% Mo. The calculated emf line for this composition lies 75% higher than the experimental subset. However, if calculated for the 46 at.% Mo composition, as shown in Fig. 4, the emf curve would then be in perfect accord with the experimental data.

The calculated Co and Mo activities in the whole composition range at 1273 and 1373 K are shown in Fig. 3. They are also in a relatively good agreement with the activity data derived from the emf measurements of [75Kat]. As discussed in sections 2.2 and 3.2, the Mo activity and the emf data from [65Dro] were not used in the assessment because they were incompatible with both the emf measurements of [75Kat] and most of the phase diagram data.

5. Conclusions

A set of optimized Gibbs energy expressions for all observed phases in the Co-Mo system was produced based on critically reviewed thermochemical and phase diagram data. The best system description was achieved with a Redlich-Kister model for the solution phases: liquid, cph and fcc (Co), bcc (Mo), compound energy formalism for the μ and σ intermetallics, and a line compound model for the ε phase.

The calculated phase diagram revealed several features not described in previous work. First, including the magnetic contribution to the Gibbs energy of fcc (Co) causes an abrupt change of the Mo solubility in fcc (Co) below T_c and predicts a miscibility gap in this phase. Second, the Co-rich phase, generally referred to as the θ phase (or Co_9Mo_4 compound), was described as the paramagnetic cph (Co) solid solution.

Several variations of the sublattice model were employed to describe the μ and σ compounds. For the μ phase they included the commonly accepted $(Co,Mo)_7(Mo)_2(Co,Mo)_4$ model, the simplified $(Co,Mo)_7(Co,Mo)_6$ description, and the relatively new $(Co)_6(Co,Mo)_1(Mo)_4(Co,Mo)_2$ model. For the σ phase, along with the traditional $(Co)_8(Mo)_4(Co,Mo)_{18}$ sublattice model, the alternative description $(Co)_{10}(Mo)_4(Co,Mo)_{16}$ was utilized, which is consistent with its crystallography. The above models were equivalent in terms of their compatibility with the other phase descriptions and in respect to an adequate representation of the experimental phase diagram and thermochemical data. This variety of descriptions was employed to facilitate compatibility with other work in the literature for similar phases and for future extrapolations to higher order systems.
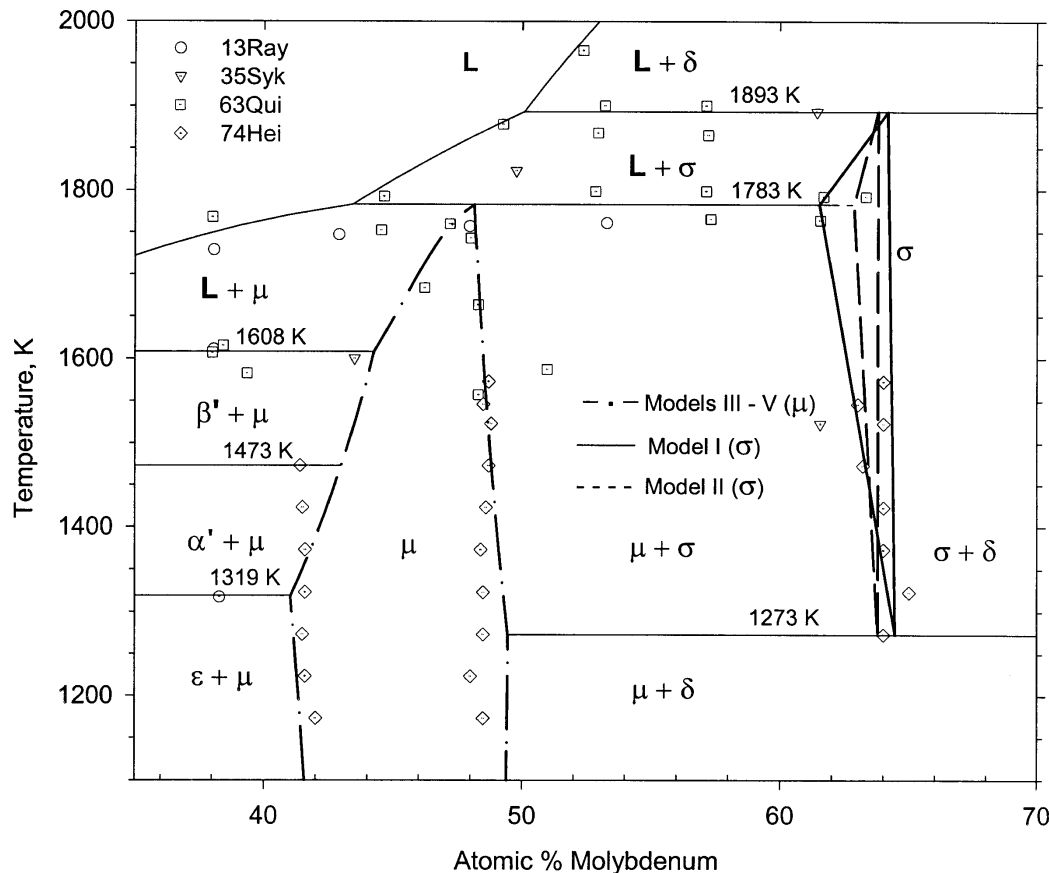
Fig. 6 Phase diagram in the vicinity of the μ and σ phases

sara and Dr. N. Dupin, L'Institut National Polytechnique de Grenoble, France, for helpful advice on the cph/θ phase modeling and for providing the list of references from the THER-MET bibliographical database.

References

13Ray: U. Raydt and G. Tammann, *Z. Anorg. Chem.,* Vol 83, 1913, p 246- 252

28Tak: T. Takei, *Kinzoku-No-Kenkyu,* Vol 5, 1928, p 364-384

32Kos: W. Köster and W. Tonn, *Z. Metallkde.,* Vol 24, 1932, p 296-299

35Syk: W.P. Sykes and H.F. Graff, *Trans. ASM,* Vol 23, 1935, p 249-285

48Red: O. Redlich and A.T. Kister, *Ind. Eng. Chem.,* Vol 40, 1948, p 345-348

53Met: A. Metcalfe, *Trans. AIME,* Vol 197, 1953, p 357-364

55Tau: K.J. Tauer and R.J. Weiss, *Phys. Rev.,* Vol 100, 1955, p 1223-1224

63For: J.B. Forsyth and M. D'Alte da Veiga, *Acta Crystallogr.,* Vol 16, 1963, p 509-512

63Qui: T.J. Quinn and W. Hume-Rothery, *J. Less-Common Met.,* Vol 5, 1963, p 314-324

65Dro: V.N. Drobyshev, T.N. Rezukhina, and L.A. Tarasova, *Russ. J. Phys. Chem.,* Vol 39, 1965, p 70-73

70Kra: W. Krajewski, J. Kruger, and H. Winterhager, *Cobalt,* Vol 48, 1970, p 120-128

74Hei: C.P. Heijwegen and G.D. Rieck, *J. Less-Common Met.,* Vol 34, 1974, p 309-314

75Gus: W. Gust, B. Predel, and S.N. Mehra, *Mater. Sci. Eng.,* Vol 21, 1975, p 131-138

75Kat: I. Katayama, M. Aoki, and Z. Kozuka, *Nippon Kinzoku Gakkai-Shi,* Vol 39, 1975, p 1210-1214

75Spe: P.J. Spencer and F.H. Putland, *J. Chem. Thermodyn.,* Vol 7, 1975, p 531-536

77Luk: H.L. Lukas, E.-Th. Henig, and B. Zimmermann, *Calphad,* Vol 1, 1977, p 225-236

78Hil: M. Hillert and M. Jarl, *Calphad,* Vol 2, 1978, p 227-238

78Kau: L. Kaufman and H. Nesor, *Calphad,* Vol 2, 1978, p 81-108

78Rez: T.N. Rezukhina and T.A. Kashina, *J Chem. Thermodyn.,* Vol 10, 1978, p 279-288

80Bre: L. Brewer, R.H. Lamoreaux , R. Ferro, R. Marazza, and K. Girgis, *Molybdenum: Physico-Chemical Properties of Its Compounds and Alloys. Atomic Energy Review,* International Atomic Energy Agency, Vienna, 1980, Special Issue No. 7, p 123-127, p 231-234

81Ind: G. Inden, *Physica,* Vol 103B, 1981, p 82-100

81Tak: T. Takayama, M.Y. Wey, and T. Nishizawa, *Trans. J. Inst. Met.,* Vol 22, 1981, p 315-325

81Sun: B. Sundman and J. Agren, *J. Phys. Chem. Solids,* Vol 42, 1981, p 297-301

82Fer: A. Fernández Guillermet, *Calphad,* Vol 6, 1982, p 127-140

82Her: S. Hertzman and B. Sundman, *Calphad,* Vol 6, 1982, 67-80

82Ind: G. Inden, *Bull. Alloy Phase Diagrams,* Vol 2, 1982, p 412-422

83And: J.-O. Andersson, *Calphad,* Vol 7, 1983, p 305-315

83Kub: O. Kubaschewski and T. Hoster, *Z. Metallkde.,* Vol 74, 1983, p 607-609

85Sun: B. Sundman, B. Jansson, and J.-O. Andersson, *Calphad,* Vol 9, 1985, p 153-190

87And: J.-O. Andersson and B. Sundman, *Calphad,* Vol 11, 1987, p 83-92

87Gus: P. Gustafson, *Metall. Trans. A,* Vol 18, 1987, p 175-188

88Fer: A. Fernández Guillermet and J.-O. Andersson, *Calphad,* Vol 12, 1988, p 9-23

89Fer: A. Fernández Guillermet, *Metall. Trans. A,* Vol 20A, 1989, p 935-955

90Hua: W. Huang, *Z. Metallkde.,* Vol 81, 1990, p 397-404

90Kat: U.R. Kattner, unpublished work, 1990

91Din: A.T. Dinsdale, *Calphad,* Vol 15, 1991, p 317-425

91Hua: W.M. Huang, *Calphad,* Vol 15, 1991, p 195-208

93Dup: N. Dupin and 1. Ansara, *J. Phase Equilibria,* Vol 14, 1993, p 451-456

93Pre: B. Predel, in *Landolt-Börnsten: Phase Equilibria, Crystallographic and Thermodynamic Data of Binary Alloys,* Group IV, Vol 5c, Springer-Verlag, Berlin, 1993, p 318-321

94Coe: G.C. Coelho, S.G. Fries, H.L. Lukas, P. Majewski, J.M. Zelaya Bejarano, S. Gama, C.A. Ribeiro, and G. Effenberg, *Proc. K. Schulze Symp. on Process. and Appl. of High Purity Refractory Metals and Alloys, 1993,* TMS, 1994, p 51-70

96Bol: A. Bolcavage and U.R. Kattner, *J. Phase Equilibria,* Vol 17, 1996, p 92-100

96Du: Y. Du and R. Schmid-Fetzer, *J. Phase Equilibria,* Vol 17, 1996, p 311-324

97Ans: I. Ansara, T.G. Chart, A. Fernández Guillermet, F.H. Hayes, U.R. Kattner, D.G. Pettifor, N.Saunders, and K. Zeng, *Calphad,* Vol 21, 1997, p 171-218

97Har: K.C. Hari Kumar, Katholieke Universiteit Leuven, private communication, 1997, cited in [97Ans]

97Kus: A. Kusoffsky and B. Jansson, *Calphad,* Vol 21, 1997, p 321-333